SUPPORTING ONLINE MATERIAL

Anomalous Brownian motion discloses viscoelasticity in the ear's mechanoelectrical-transduction apparatus

Andrei S. Kozlov*, Daniel Andor-Ardó*, and A. J. Hudspeth

Howard Hughes Medical Institute and Laboratory of Sensory Neuroscience, The Rockefeller University, 1230 York Avenue, New York, New York 10065, USA

Section 1. The relation between a hair bundle's fluctuations and its mechanical properties

In order to compare our data with model predictions, we require a relation between the statistics of hair-bundle motion and the parameters of the model. From a biophysical model comprising a network of linear springs and dashpots as well as nonlinear channels we may obtain the mean square displacement and power spectrum. One way to do this is to simulate all the components of the model, including thermal forces, and analyze the results as if they were experimental data. If the system is in thermal equilibrium at a stable fixed point, however, the model's linear response function provides the power spectrum directly through the fluctuation-dissipation theorem. Passive microrheology exploits the fact that the reverse is also true: we may estimate the linear response function of the system from experimental noise data.

The dynamics of a small deviation $\delta\mathbf{x}$ of an N-dimensional system from a fixed point as a result of a force $\mathbf{f}$ may be written as

$$\Lambda\delta\dot{\mathbf{x}}(t) + \mathbf{K}\delta\mathbf{x}(t) = \mathbf{f}(t), \tag{S1}$$

in which the phenomenological drag coefficient Λ and stiffness $\mathbf{K}$ are N-by-N matrices determined by the model and the location of the fixed point. This relation also results from a

linear noise approximation of the master equation[1]. The force $\mathbf{f}$ is thermodynamically conjugate to the extensive variable $\delta\mathbf{x}$ such that their product is an energy.

After Fourier transformation, we can rewrite Eq. S1 as

$$\mathbf{Z}(\omega)\delta\mathbf{x}(\omega) = \mathbf{f}(\omega), \tag{S2}$$

in which $\mathbf{Z}(\omega)$ is the complex impedance matrix. The fluctuation-dissipation theorem allows us to connect the linear response function of the system with its equilibrium fluctuations. The theorem gives the power spectrum $\mathbf{S}(\omega) = \int_{-\infty}^{\infty} \langle \mathbf{x}(t)\mathbf{x}(t)^T \rangle e^{i\omega t} dt$ as

$$\mathbf{S}(\omega) = -\frac{2k_B T \,\mathrm{Im}[\chi(\omega)]}{\omega}, \tag{S3}$$

in which the matrix $\chi(\omega) = \mathbf{Z}(\omega)^{-1}$ is the linear response function, k_B the Boltzmann constant, and T the temperature. In this way we can compare theoretically predicted power spectra with those measured experimentally (Fig. 4).

We can also work backward from the experimental data. For instance, if we estimate $\mathbf{S}(\omega)$ from the data, we can use Eq. S3 directly to calculate $\mathrm{Im}[\chi(\omega)]$. Because the linear response function $\chi(t)$ must be causal, we can then obtain its real part with the Kramers-Kronig relations (see below).

To understand the mechanical properties of the system, we calculate the reciprocal of $\chi(\omega)$. The resulting complex spring constant $G(\omega) = 1/\chi(\omega)$, whose real and imaginary parts determine respectively the material's frequency-dependent elasticity and viscosity, is proportional to the material's shear modulus. Our figures can be interpreted as plots of the shear modulus with the geometric factor set to identity.

Section 2. Control experiments and statistical quantification of the data

Equilibrium Gaussian properties

Because several mechanisms can in principle generate anomalous, subdiffusive behavior, we considered the time reversibility and Gaussian nature of the process in order to narrow the set of

possible models. The records are time-reversible on short timescales[2,3] (Fig. S1). We next tested for the Gaussian property of the process and found that bundle fluctuations deviate from a Gaussian distribution only on long timescales and during spontaneous oscillation (Fig. S2). The bundles' movements at frequencies above 100 Hz could therefore be described as an equilibrium Gaussian process. These findings are in accord with a previous analysis in which hair bundles were found to display equilibrium fluctuations at frequencies above those of their oscillations[4].

The fact that only the slow oscillatory regime is non-Gaussian and non-reversible suggests that non-equilibrium processes are limited to long timescales, leaving time for fast processes to equilibrate. To confirm that the faster motion is purely thermal, we performed experiments with agents that arrest cellular metabolism and thus bring cells to thermal equilibrium. To deplete cells of ATP, we used sodium azide (NaN_3) and carbonyl cyanide *m*-chlorophenylhydrazone (CCCP) to interrupt oxidative phosphorylation and deoxyglucose to block glycolysis. NaN_3 has been shown to block the active processes in living hair cells[5] and a combination of CCCP and deoxyglucose has been used to deplete hair cells of ATP[6]. Under these conditions we consistently observed subdiffusive behavior (Fig. 1).

To exclude the possibility that the subdiffusive mean square displacement and power spectra were artifacts of the recording environment or of data processing, we recorded from preparations expected to perform ordinary diffusion. Damaged hair bundles often splay to reveal individual stereocilia and kinocilia that are completely disconnected from their neighbors. These objects displayed ordinary diffusion and Lorentzian power-law scaling of the power spectrum with a slope of -2 in logarithmic coordinates (Fig. 1). In contrast, no combination of parameters in Eq. 3 of the main text, which describes fluctuations in the canonical gating-spring model, can even roughly approximate the high-frequency slope of the power spectrum of an intact bundle. The inadequacy of a Lorentzian fit to these high-frequency spectra has been noted previously[7]. These control experiments emphasize the systematic and significant deviation of the intact hair bundles' random movements from ordinary diffusion.

To exclude the possibility that additive noise contributed to the inadequacy of a Lorentzian fit, we performed two controls. First, we recorded from a micrometer-size bead immobilized in agar to directly measure background additive noise. The background noise was much smaller than hair-bundle fluctuations at all frequencies and was flat above 2 kHz (Fig. S3). Second, we performed recordings with a bandwidth extended to 50 kHz. When added to the signal, white noise must produce a spectrum that is concave in logarithmic units at frequencies for which it appears subdiffusive and flat at higher frequencies. Our extended-bandwidth recordings (Fig. S4) underscore the fact that the experimental power spectra are not concave. No level of additive white noise can produce our observed spectra, which are instead convex. This conclusion is corroborated by our maximum-likelihood fit of the data, in which we allowed for the possibility of additive noise.

Finally, to show in an essentially non-parametric way that records from BAPTA-treated cells cluster with those from isolated stereocilia, whereas cells with blocked mechanotransduction channels cluster with thermalized and control cells, we projected all the records from all hair bundles onto a two-dimensional space determined through principal-components analysis (Fig. S5). In this representation, the first principal component captured 99 % of the variance.

Maximum-likelihood fit of data

To accurately fit our data, we formed a generative statistical model consisting of a Gaussian process with Mittag-Leffler covariance and maximized the likelihood of the parameters given the data. This procedure is distinct from least-squares fitting of curves to plots of either mean square displacement or power spectral density. The estimates of parameter values obtained by maximum likelihood can subsequently be used to plot model-generated mean square displacement and power spectral density curves.

For a Gaussian process of zero mean and covariance matrix C, the log-likelihood for a vector of observations x is

$$\begin{aligned} L &= \ln\left[P(x \mid C)\right] \\ &= -\tfrac{1}{2} x^T C^{-1} x - \tfrac{1}{2} \ln\left|2\pi C\right|. \end{aligned} \tag{S4}$$

In our case matrix C is parameterized and takes the form

$$C = C_{\mathrm{ML}}(\alpha, \tau) + \mathbf{I}\sigma^2, \tag{S5}$$

in which α and τ are parameters of the Mittag-Leffler function, $\mathbf{I}$ is the identity matrix, and σ^2 is the variance of any additive experimental noise. C_{ML} is a stationary covariance matrix whose element at row t and column t' is defined by

$$C_{\mathrm{ML}}(t, t') = C_{\mathrm{ML}}(|t - t'|) \propto E_\alpha\left[-(|t - t'| / \tau)^\alpha\right], \tag{S6}$$

in which $E_\alpha[z]$ is the Mittag-Leffler function.

The primary algorithmic challenge is to optimize the parameters without having to store the elements of C or to calculate directly the inverse and determinant in Eq. S4. Owing to the stationary structure of C, however, we may use Fourier transforms to approximately calculate $x^T C^{-1} x$. The Fourier transform of the Mittag-Leffler correlation function is given by

$$\tilde{C}_{\mathrm{ML}}(\omega) \propto \mathrm{Re}\left[\frac{1}{i\omega(1 + (i\omega\tau)^{-\alpha})}\right]. \tag{S7}$$

We calculate the required power spectral estimates of the data x by the multitaper method[8]. Once in the Fourier domain, we limit our fitting routine to data from hair bundles in the frequency range between 400 Hz and 10 kHz. Restricting the data in this way is tantamount to using a prior that professes skepticism about the ability of the model to fit data for frequencies outside this range. Finally, we estimate the parameters α, τ and σ^2 by numerically maximizing L. The value of the overall power density of the data is absent from the optimization because, as a unit of measure of x, it is arbitrary and is scaled out. Confidence intervals are estimated by evaluating the diagonal of the Hessian of L at the optimal parameter values. After fitting our data, the additive noise parameter σ^2 assumes a value of zero within machine precision, indicating that the term $\mathbf{I}\sigma^2$ in Eq. S5 is negligibly small.

In general, when dealing with fractional Brownian processes, one must be careful in moving between a description of a continuous process and the discrete representation found in actual data. In particular, the discretized autocorrelation function of a continuous process is not the autocorrelation function of a discretized version of the process. Owing to the limited frequency band used for fitting, no such problem arises in this particular instance.

Estimating viscoelastic moduli

The mechanical properties of a viscoelastic material can be described by a frequency-dependent complex shear modulus, $G^*(\omega)$, which can be obtained as follows. First, using the fluctuation-dissipation theorem for systems at thermodynamic equilibrium, one can calculate the imaginary part of the linear response function, $\chi''(\omega) \equiv \mathrm{Im}[\chi(\omega)]$, from the power spectrum of thermal fluctuations, $S(\omega)$,

$$\chi''(\omega) = -\frac{\omega}{2k_B T} S(\omega). \tag{S8}$$

For causal systems, the imaginary part of the response function is related to the real part through the Kramers-Kronig relations: if one knows $\chi''(\omega)$ over a sufficiently broad frequency range, one can reconstruct the entire complex response function $\chi(\omega) = \chi'(\omega) + i\chi''(\omega)$ over that range. The response function can then be used to obtain the complex shear modulus $G^*(\omega)$ through a generalized Stokes-Einstein relation for a probe particle of radius a,

$$G^*(\omega) = \frac{1}{6\pi a \chi(\omega)}. \tag{S9}$$

The complex shear modulus $G^*(\omega) = G'(\omega) + iG''(\omega)$ comprises the storage modulus and the loss modulus, which are also interdependent through Kramers-Kronig relations. The generalized Stokes-Einstein relation assumes no-slip boundary conditions; a continuum, isotropic, and incompressible material; and the absence of inertia. This method has been used successfully to estimate the moduli from measurements of thermal motions of microscopic particles embedded in a complex viscoelastic milieu[9]. In our case, however, the exact value of

the geometrical prefactor in the denominator is unknown and thus only the frequency scaling, but not the absolute values, of the reported quantities is accurate.

Because the Kramers-Kronig integrals are exact only when evaluated over infinite frequency space, which is impossible with finite data, the moduli obtained with this method may suffer from errors that grow at the extrema of the integration interval. We therefore employed a second method that is more robust at the limits of a finite frequency range[10]. This approach does not rely explicitly on the Kramers-Kronig relations; instead, it algebraically expands the mean square displacement around a frequency of interest, truncates the expansion, and uses the slope of the resulting power law to obtain the local scaling exponent. Provided that the frequency scaling is smooth, this method performs well at the limits of the frequency range.

Using these complementary methods to estimate the scaling of the viscoelastic moduli, we obtained a good agreement between them. As expected, the second method was more accurate at the high- and low-frequency limits.

Section 3. Modeling and simulating viscoelasticity in the hair bundle

Model and mode decomposition

The transduction channels lie in series with the tip links (Fig. S6). Their gating state is captured by the binary variable $s_j \in \{0,1\}$ for channel $j \in \{1...N\}$. The opening of a channel shortens the associated gating spring by the gating distance *d*. In series with the gating spring we hypothesize additional viscoelastic components that together have a general linear response whose structure and magnitude are to be determined. For a given tension f_j in a particular gating spring *j*, the opening and closing rate constants of the channels are determined by a free energy that is linear in the force[11,12],

$$k_{\pm}^{(j)} = k_{\pm}(f_j) = \exp\left[E_0 - (\Delta - \tfrac{1}{2} \pm \tfrac{1}{2})(E_1 - \beta d f_j)\right], \qquad \text{(S10)}$$

in which $\beta = 1/k_B T$ and Δ is the proportion of the free-energy difference that gating adds to the barrier. The constants E_0 and E_1 are determined by the mean open probability and mean open time, which are respectively

$$p^{(j)} = p(f_j) = \frac{1}{1 + \frac{k_-}{k_+}} = \frac{1}{1 + \exp\left(E_1 - \beta d f_j\right)} \tag{S11}$$

and

$$\tau(f_j) = \frac{1}{k_+(f_j) + k_-(f_j)}. \tag{S12}$$

The tension f_j depends on the instantaneous state of the channel s_j, the bundle's position $X(t)$, and the internal degrees of freedom of the series viscoelastic components. Although we do not know the molecular composition of these series viscoelastic components, mode decomposition provides an effective way to model their fractal behavior.

Adjacent pairs of stereocilia along a hair bundle's axis of mechanical sensitivity are connected by tip links, which are in turn coupled through the other components of the gating springs to mechanoelectrical-transduction channels[13]. The bundle displacement $X(t)$ projects onto each obliquely oriented tip link through a geometric factor $\gamma \sim 0.14$ and the tension in the tip link influences the stereocilia through the same factor. The gating spring has spring constant κ and the viscoelastic components have a general linear response $g(t)$, whose structure and magnitude are to be determined. The tension f_j in a gating spring depends on the history of channel openings through the memory kernel $q_j(t)$:

$$f_j = \int_{-\infty}^{t} q_j(t - t')\left[X(t') - s_j(t')d\right]dt'. \tag{S13}$$

The viscoelastic linear response $g(t)$ affects $q_j(t)$ because $q_j(t)$ is the memory kernel related to the linear response function $\frac{1}{\kappa} + g(t)$.

We may decompose the bundle's response to the stereociliary and thermal forces into a series of modes. A simple viscoelastic mode, comprising a spring with a spring constant κ and a dashpot with a friction coefficient ξ in parallel, has an exponential response with time constant

$\tau = \xi/\kappa$. When there are multiple modes in series the linear responses sum, so in the Fourier domain we have

$$\tilde{g}(\omega) = \sum_m \frac{1}{\kappa_m + i\omega\xi_m}. \tag{S14}$$

For the calculations in this paper we used the mode structure of the worm-like chain[14], for which $\xi_m = \xi^{(0)}$ for all modes m and $\kappa_m = m^4\kappa^{(0)}$. A finite sum over m quickly approximates subdiffusion with $\alpha = 3/4$. We found that a sum in which m runs from 1 to 3 yields subdiffusive behavior over more than a decade in frequency and was sufficient for all the calculations in this paper.

Simulations

Using a Langevin scheme we simulated $X(t)$, $s_i(t)$, and the internal degrees of freedom associated with the modes of $g(t)$. The simulations generated synthetic data that could be analyzed by the methods used for experimental data and compared directly to those results. Each viscoelastic mode (Eq. S14) is represented as an Ornstein-Uhlenbeck process with independent, Gaussian thermal noise of standard deviation $\sqrt{2k_BT\xi_m}$. Each channel with the associated tip link is considered separately, with the tension in the gating spring determining the opening or closing rate (Eq. S10). The resulting rate determines a channel's probability of changing its state $s_i(t)$ at the end of a given time step. The forces arising through the channels are summed and added to the bulk elastic and damping forces on the bundle. Along with the fluid-dependent thermal force $\sqrt{2k_BT\lambda}$ there is a constant biasing force on the bundle that without loss of generality ensures that the fixed point of $X(t)$ is such that the mean open probability of the channels (Eq. S11) matches the desired value. The simulation time step is chosen to be much smaller than the mean open time of the channels at this open probability.

Linear noise approximation

Thermodynamic equilibrium and linearization of the dynamics about a fixed point allow us to approximate analytically the linear response and power-spectral density of a hair bundle and its channels. This approach facilitates the search for parameter values to fit the model to data, allows us to take limits, and clarifies the relationship between bundle motion and channel response.

Using the switching rates specified by Eq. S10 we can define a master equation over the state of the channels. The number of open channels at a given instant is $n(t) = \sum_{i=1}^{N} s_i(t)$. In the linear noise approximation[1] we may write the dynamics in terms of the mean bundle position X and the mean number n of open channels[15]. Linearized and in the Fourier domain, $\tilde{X}$ and $\tilde{n}$ are related to their conjugate thermal forces $\tilde{F}$ and $\tilde{E}$ by the matrix equation

$$\mathbf{Z}\begin{bmatrix}\tilde{X}\\ \tilde{n}\end{bmatrix} = \begin{bmatrix}\tilde{F}\\ \tilde{E}\end{bmatrix}, \tag{S15}$$

in which $\mathbf{Z}$ is a complex impedance matrix

$$\mathbf{Z} = \begin{bmatrix}k + \bar{k} + i\omega\lambda & -z\\ -z & (1 + i\omega\tau)\varepsilon\end{bmatrix} \tag{S16}$$

that satisfies Onsager reciprocity. The stiffnesses k and $\bar{k}$ are respectively the elastic contributions of the stereociliary pivots and the sum of the viscoelastic responses of the channel complexes in the bundle's frame of reference. The force associated with opening the channels is $z = d\bar{k}$. Thermal fluctuations in n lead to an energy constant $\varepsilon = \frac{k_B T}{N p_O (1-p_O)}$ determined by the value of the open probability p_O at the fixed point. Lastly, the mean open time of the channels $\tau = 1/(k_+ + k_-)$ is also evaluated at the fixed point.

The linear response matrix χ of the system is given by the matrix inverse of $\mathbf{Z}$:

$$\chi = \mathbf{Z}^{-1} = \frac{1}{(k + \bar{k} + i\omega\lambda)(1 + i\omega\tau)\varepsilon - z^2}\begin{bmatrix}(1 + i\omega\tau)\varepsilon & z\\ z & k + \bar{k} + i\omega\lambda\end{bmatrix}. \tag{S17}$$

By the fluctuation-dissipation theorem, the power-spectral density follows from the imaginary part of the linear response,

$$\mathbf{S}(\omega) = \frac{-2k_{\mathrm{B}}T\,\mathrm{Im}\left[\chi(\omega)\right]}{\omega}. \tag{S18}$$

The fluctuation power spectrum of variable $X(t)$ is determined by the S_{XX} component of matrix **S**. When the viscoelastic components are absent, $\bar{k} = N\gamma^2\kappa$, and the response simplifies to

$$S_{XX}^{\mathrm{elastic}} = 2k_{\mathrm{B}}T\frac{\lambda(1+\tau^2\omega^2)+\tau z^2/\varepsilon}{\left[(k+\bar{k}-\lambda\tau\omega^2)-z^2/\varepsilon\right]^2+\left[\lambda+(k+\bar{k})\tau\right]^2\omega^2}\ . \tag{S19}$$

When the channels are blocked, equivalent to the limit $\tau \to \infty$, the spectrum becomes

$$S_{XX}^{\mathrm{blocked}} = \lim_{\tau\to\infty} S_{XX}^{\mathrm{elastic}} = \frac{2k_{\mathrm{B}}T\lambda}{(k+\bar{k})^2+\lambda^2\omega^2}. \tag{S20}$$

When the channels gate instantaneously, equivalent to the limit $\tau \to 0$, the spectrum becomes

$$S_{XX}^{\mathrm{instantaneous}} = \lim_{\tau\to 0} S_{XX}^{\mathrm{elastic}} = \frac{2k_{\mathrm{B}}T\lambda}{(k+\bar{k}-z^2/\varepsilon)^2+\lambda^2\omega^2}, \tag{S21}$$

in which the phenomenon of gating compliance can be observed in the decline of the stiffness from $\left(k+\bar{k}\right)$ to $\left(k+\bar{k}-z^2/\varepsilon\right)$.

Calculations based on the linear noise approximation agree well with the results of simulations (Fig. 2). Both approaches demonstrate the effect of channel clatter and the fact that it is masked by the inclusion of series viscoelastic elements. In both cases the model can be seen to satisfy our three requirements: high-frequency subdiffusion, subdiffusive channel block, and reversion to ordinary diffusion upon tip-link scission.

Parallel coupling

The general linear response, including both series coupling *g* and parallel coupling *h*, is given in full by

$$\begin{aligned} i\omega\lambda\tilde{X} &= -(k+N\gamma^2[(\kappa^{-1}+\tilde{g})^{-1}+\tilde{h}^{-1}])\tilde{X}+N\gamma^2(\kappa^{-1}+\tilde{g})^{-1}\tilde{n}+\tilde{F},\\ i\omega\varepsilon\tau\tilde{n} &= -\varepsilon\tilde{n}+N\gamma^2(\kappa^{-1}+\tilde{g})^{-1}\tilde{X}+\tilde{E}. \end{aligned} \tag{S22}$$

Although we have focused on *g*, *h* may actually play an important role as well. To demonstrate the effect of parallel viscosity, we can consider the situation in which $\tilde{g}=0$ and it is $\tilde{h}$ that imposes multiple timescales of relaxation. This arrangement is also able to explain subdiffusion and to reduce the effects of channel viscosity (Fig. S7).

Channel block in the canonical model

It is straightforward to calculate the effect of blocking transduction channels in the canonical model (Fig. S6*A*) in which there are no viscoelastic modes in series or parallel with the transduction complex, so $g(t) = h(t) = 1$. When the channels are unable to gate, the gating springs are coupled directly to hair-bundle position and the force-balance equation is particularly simple. In the Fourier domain,

$$(i\omega\lambda + k + N\gamma^2\kappa)\tilde{X}(\omega) = \tilde{F}(\omega) \ , \tag{S23}$$

in which $\tilde{F}(\omega)$ is an external force. The power spectrum of thermal fluctuations is Lorentzian in form,

$$S(\omega) = \frac{2k_{\mathrm{B}}T\lambda}{(k + N\gamma^2\kappa)^2 + \lambda^2\omega^2} \ , \tag{S24}$$

with a corner frequency equal to $(k + N\gamma^2\kappa)/(2\pi\lambda)$. The resulting stochastic behavior represents an Ornstein-Uhlenbeck process that displays ordinary diffusion.

Section 4. Tip links as a source of viscoelasticity

One of several mechanisms put forward in the main text as a possible explanation for the viscoelastic component involves viscoelastic modes reflecting multiple timescales of protein motion.

To estimate the frequency range of transversal fluctuations, we first obtain the relaxation time τ for the lowest transversal mode of a semiflexible polymer that has the dimensions of a tip link. We do not imply by this that the tip link *per se* is the gating spring, nor that it alone is responsible for the viscoelastic behavior of the hair bundle as a whole. The link is merely the longest known element in the mechanotransduction chain and the only polymer connected to a pair of stereocilia that is oriented appropriately to interact with the coherent, shearing mode of stereociliary motion.

We apply the formula[16]

$$\tau = \frac{4\eta L^4}{\pi^3 \kappa \ln(L/\pi a)}, \tag{S25}$$

in which L is the contour length of the polymer, a its diameter, η the fluid's viscosity, and κ the bending rigidity given by $\kappa = k_B T L_p$, in which L_p is the persistence length. Taking the length of the heterotetramer[17] of cadherin-23 and protocadherin-15 as 170 nm and its diameter as 9 nm, and using the broad range 10–100 nm for the persistence length based on the observation of curled, detached tip links[18], we estimate a relaxation frequency for the first mode between 950 Hz and 9.5 kHz. Note that if the effective viscosity is locally elevated by the presence of solid boundaries such as stereocilia, this range is proportionally shifted to lower frequencies. As a control we can calculate the stiffness of a polymer that has these mechanical properties and the Young's modulus of cadherins[19] and that is subjected to several piconewtons of prestress expected from the activity of myosin motors[20]. Using a worm-like-chain model with prestress[21], we obtain a stiffness on the order of 1 $mN \cdot m^{-1}$, well within the range of values for the stiffness of the sound-transmitting elastic elements reported in the literature. Although the value for the stiffness of a tip link estimated from the crystal structure of cadherin-23 repeats is fifty times as great[22], the two models are drastically different, are based on different sets of assumptions, and can hardly be compared. Our estimation is purely statistical, rather than based on structural information, and does not bear on the question whether the tip link is the gating spring. It serves only as a check of whether the worm-like-chain model with prestress can produce a meaningful order-of-magnitude value for the stiffness that we use in the estimation of the mode-relaxation frequency.

Because of the conservation of contour length, transverse fluctuations of a polymer must alter the molecule's end-to-end distance[23]. The scaling of these fluctuations may ultimately be a consequence of the geometrical complexity of proteins. Fractal-like geometries, which are generic features of proteins and even of simpler peptides, generate complex dynamics that can be described by a generalized Langevin equation with a Mittag-Leffler decay of the correlation

function[24,25]. In fact, a hierarchical arrangement of springs and dashpots has traditionally been used to model the viscoelastic behavior of polymers[26].

Heterogeneous distribution of modes

In the models constructed thus far we have assumed that each transduction element, the complex of a tip link and the associated channels, has approximately the same properties. We have also hypothesized that each tip-link complex responds with multiple modes—usually three—in order to produce subdiffusive behavior. It is also possible to achieve subdiffusion by allowing the frequency of the modes to vary from tip link to tip link. A single viscoelastic mode is ordinarily insufficient to yield smooth subdiffusive behavior. When the frequency of a single viscoelastic mode varies systematically across an ensemble of channels, however, the result is subdiffusive, albeit with a power spectrum slightly different from that of the homogeneous model (Fig. S8).

References

1. van Kampen, N. G. (2007). Stochastic Processes in Physics and Chemistry (Elsevier, Amsterdam, The Netherlands, third edition).
2. Steinberg, I. (1986). On the time reversal of noise signals. Biophys. J. 50, 171–179.
3. Kou, S. C. & Xie, X. S. (2004). Generalized Langevin equation with fractional Gaussian noise: Subdiffusion within a single protein molecule. Phys. Rev. Lett. 93, 180603-1–180603-4.
4. Martin, P., Hudspeth, A. J. & Jülicher, F. (2001). Comparison of a hair bundle's spontaneous oscillations with its response to mechanical stimulation reveals the underlying active process. Proc. Natl. Acad. Sci. USA 98, 14380–14385.
5. Pelling, A. E., Sehati, S., Gralla, E. B., Valentine, J. S. & Gimzewski, J. K. (2004). Local nanomechanical motion of the cell wall of *Saccharomyces cerevisiae*. Science 305, 1147–1150.

6. Puschner, B. & Schacht, J. (1997). Energy metabolism in cochlear outer hair cells in vitro. Hear. Res. 114, 102–106.
7. Denk, W., Webb, W. W. & Hudspeth, A. J. (1989). Mechanical properties of sensory hair bundles are reflected in their Brownian motion measured with a laser differential interferometer. Proc. Natl. Acad. Sci. USA 86, 5371–5375.
8. Percival, D. B. & Walden, A. T. (1993). Spectral Analysis for Physical Applications: Multitaper and Conventional Univariate Techniques. (Cambridge University Press. Cambridge, UK).
9. Gittes, F., Schnurr, B., Olmsted, P. D., MacKintosh, F. C. & Schmidt, C. F. (1997). Microscopic viscoelasticity: shear moduli of soft materials determined from thermal fluctuations. Phys. Rev. Lett. 79, 3286–3289.
10. Mason, T. G. (2000). Estimating the viscoelastic moduli of complex fluids using the generalized Stokes-Einstein equation. Rheol. Acta 39, 371–378.
11. Corey, D. P. & Hudspeth, A. J. (1983). Kinetics of the receptor current in bullfrog saccular hair cells. J. Neurosci. 3, 962–976.
12. Sachs, F. & Lecar, H. (1991). Stochastic model for mechanical transduction. Biophys. J. 59, 1143–1145.
13. Hudspeth, A. J. (1989). Mechanoelectrical transduction by hair cells of the bullfrog's sacculus. Prog. Brain Res. 80, 129–135.
14. Gittes, F. & MacKintosh, F. C. (1998). Dynamic shear modulus of a semiflexible polymer network. Phys. Rev. E 58, R1241–R1244.
15. Bialek, W. & Setayeshgar, S. (2005). Physical limits to biochemical signaling. Proc. Natl. Acad. Sci. U.S.A. 102, 10040–10045.
16. Caspi, A., Granek, R. & Elbaum, M. (2002). Diffusion and directed motion in cellular transport. Phys. Rev. E 66, 011916-1–011916-12.
17. Kazmierczak, P. et al. (2007). Cadherin 23 and protocadherin 15 interact to form tip-link filaments in sensory hair cells. Nature 449, 87–91.

18. Auer, M. et al. (2008). Three-dimensional architecture of hair-bundle linkages revealed by electron-microscopic tomography. J. Assoc. Res. Otolaryngol. 9, 215–224.
19. Sotomayor, M. & Schulten, K. (2008). The allosteric role of the Ca^{2+} switch in adhesion and elasticity of C-cadherin. Biophys. J. 94, 4621–4633.
20. Jaramillo, F. & Hudspeth, A. J. (1993). Displacement-clamp measurement of the forces exerted by gating springs in the hair bundle. Proc. Natl. Acad. Sci. USA 90, 1330–1334.
21. Odijk, T. (1995). Stiff chains and filaments under tension. Macromolecules 28, 7016–7018.
22. Sotomayor, M., Weihofen, W. A., Gaudet, R. & Corey, D. P. (2010). Structural determinants of cadherin-23 function in hearing and deafness. Neuron 66, 85–100.
23. Everaers, R., Julicher, F., Ajdari, A. & Maggs, A. C. (1999). Dynamic fluctuations of semiflexible filaments. Phys. Rev. Lett. 82, 3717–3720.
24. Granek, R. & Klafter, J. (2005). Fractons in proteins: can they lead to anomalously decaying time autocorrelations? Phys. Rev. Lett. 95, 098106-1–098106-4.
25. Neusius, T., Daidone, I., Sokolov, I. M. & Smith, J. C. (2008). Subdiffusion in peptides originates from the fractal-like structure of configuration space. Phys. Rev. Lett. 100, 188103-1–188103-4.
26. Schiessel, H. & Blumen, A. (1993). Hierarchical analogs to fractional relaxation equations. J. Phys. A-Math. Gen. 26, 5057–5069.

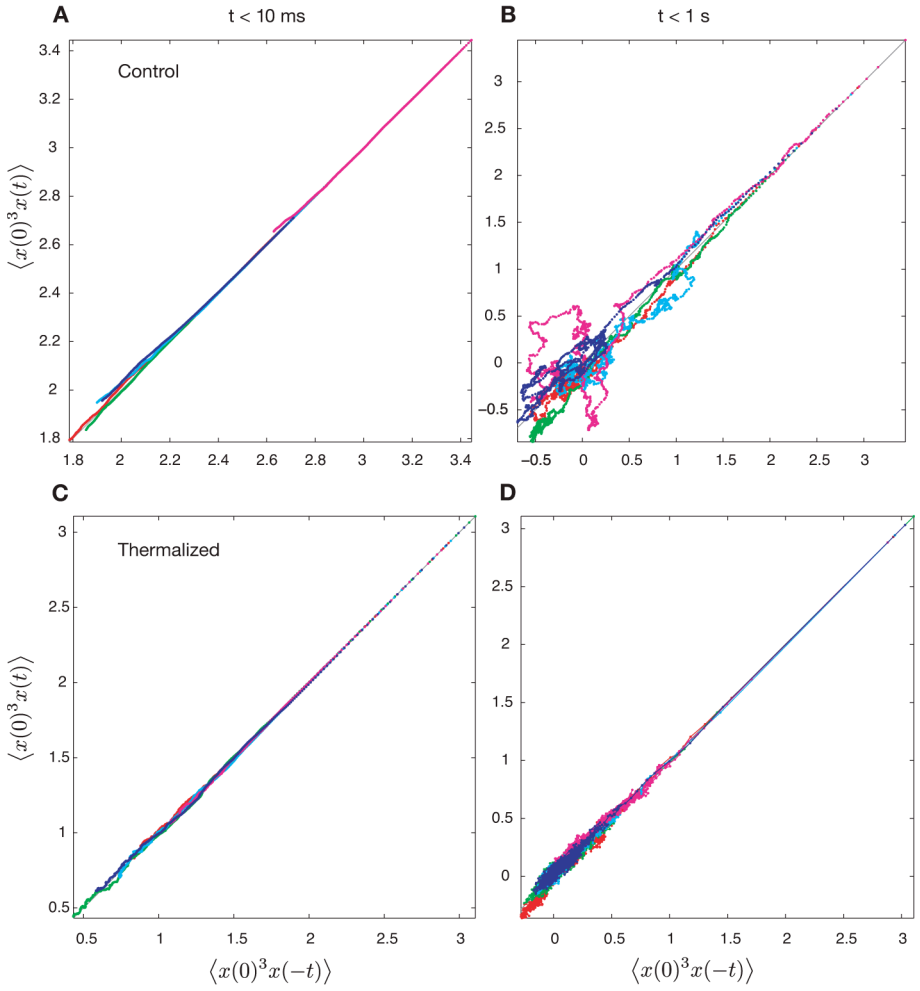

Figure S1. Analysis of time reversibility of traces. By generalizing the autocorrelation function to ensemble averages of differing powers of the signal at different times, we may detect a change in statistical properties of the noise signal upon time reversal[2]. For instance, the ensemble averages $\rho_{\pm}(t) = \langle x(0)^3 x(\pm t) \rangle$ are equal if the signal is time reversible. We computed $\rho_{\pm}(t)$ for living and oscillating hair cells (top row) and for cells at thermodynamic equilibrium (bottom row). The oscillations of live cells are relatively slow, with a period of 10–200 ms. Data that lie on the diagonal, as in panels *A*, *C* and *D*, are consistent with equilibrium thermal processes. Restricting the analysis to delays less than 10 ms (left column) allows both living and dead cells to satisfy the equilibrium condition. At longer delays (right column) the non-equilibrium signature of a living cell becomes apparent (panel *B*).

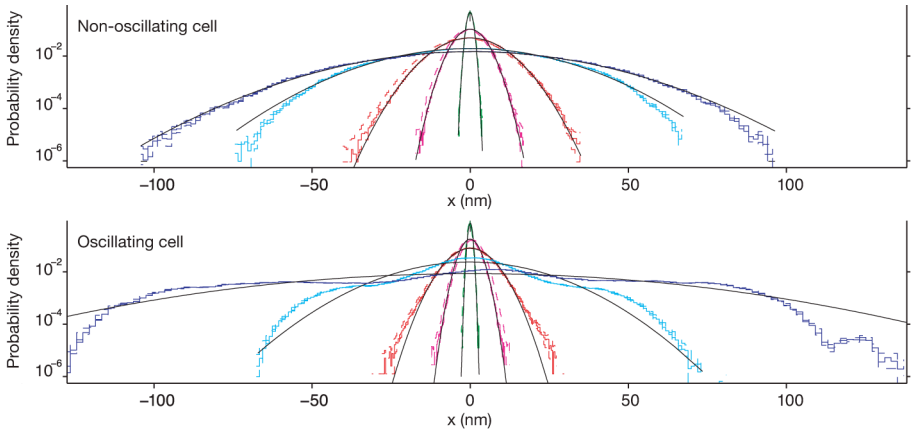

Figure S2. Analysis of the Gaussian property for oscillating and non-oscillating hair bundles. A process is Gaussian if the joint distribution of any variables is jointly normal and can be described fully by a covariance matrix. For instance, the displacement x should follow the probability distribution $P(x \mid C) = \exp(\frac{1}{2} x^T C^{-1} x)/Z(C)$ for an autocorrelation matrix C. In particular, the distribution of displacements for any given time lag should be Gaussian. These log-linear plots show the distributions of x conditioned on various lag times τ. The data generally fit Gaussian distributions, which are represented by parabolas. The statistic $\alpha_2 = \left\langle x^4 \right\rangle \Big/ 3\left\langle x^2 \right\rangle^2 - 1$ quantifies how well higher cumulants of the data can be predicted by lower-order cumulants; a truly Gaussian process exhibits a value of zero. From the narrowest to the broadest curve in the upper panel, the successive time lags and statistical values are: t = 0.1 ms, α_2 = 0.008; t = 1 ms, α_2 = 0.008; t = 10 ms, α_2 = 0.024; t = 100 ms, α_2 = -0.061; and t = 1 s, α_2 = -0.039. In the lower panel, the statistics for the same time lags are α_2 = 0.009, α_2 = 0.017, α_2 = 0.12, α_2 = 0.50, and α_2 = -0.16.

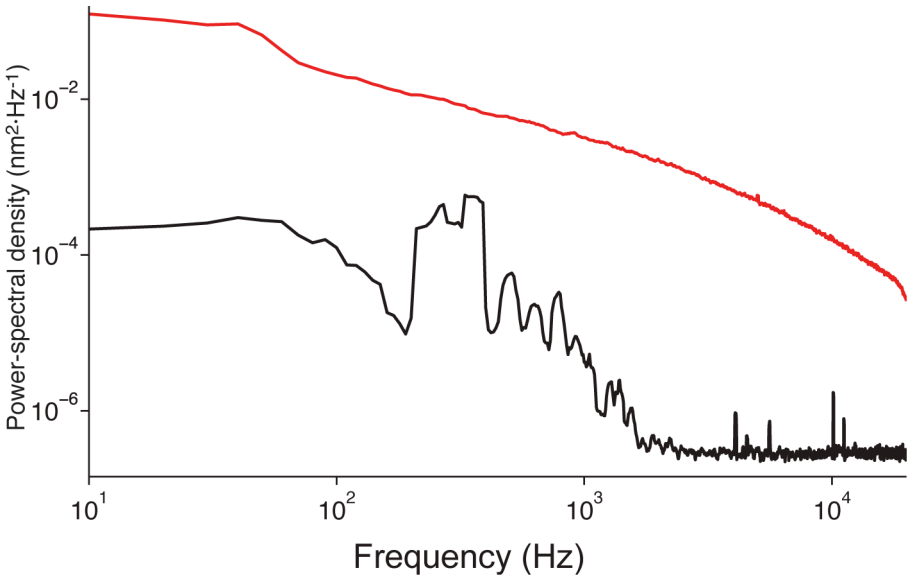

Figure S3. Characterization of additive instrumental noise.

The apparent motion of a micrometer-size glass bead embedded in a block of agar (black) displays a much smaller spectral power than does the motion of a hair bundle (red). The former spectrum provides an estimate of the background noise in the recording apparatus.

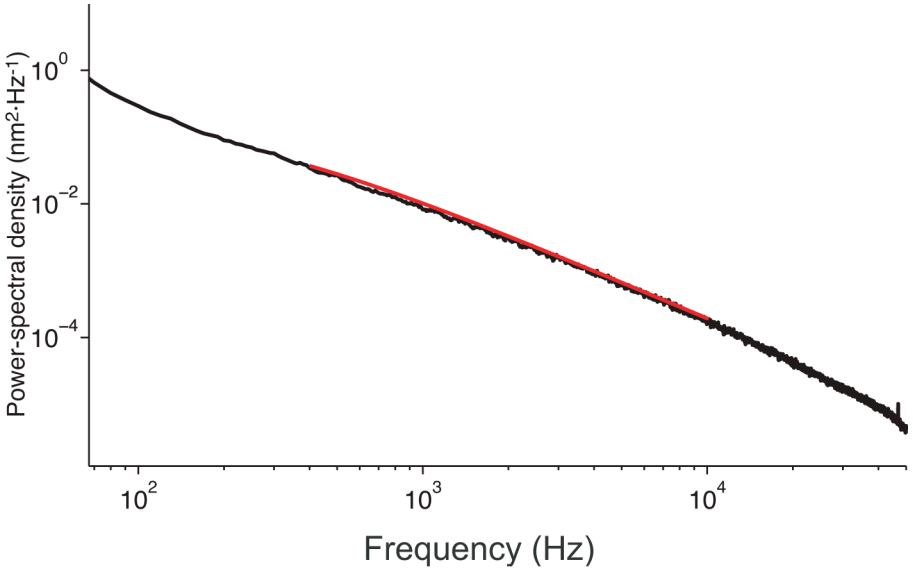

Figure S4. Demonstration of convexity of power spectra at high frequency.

The experimental record (black) was obtained with the low-pass filter's corner frequency set to 50 kHz and the signal was sampled at 5 μs intervals. The power spectrum shows no sign of flattening at high frequencies, which would have to occur if additive noise with a flat spectrum were significant. A Mittag-Leffler function is superimposed with $\alpha = 0.82 \pm 0.01$ (red).

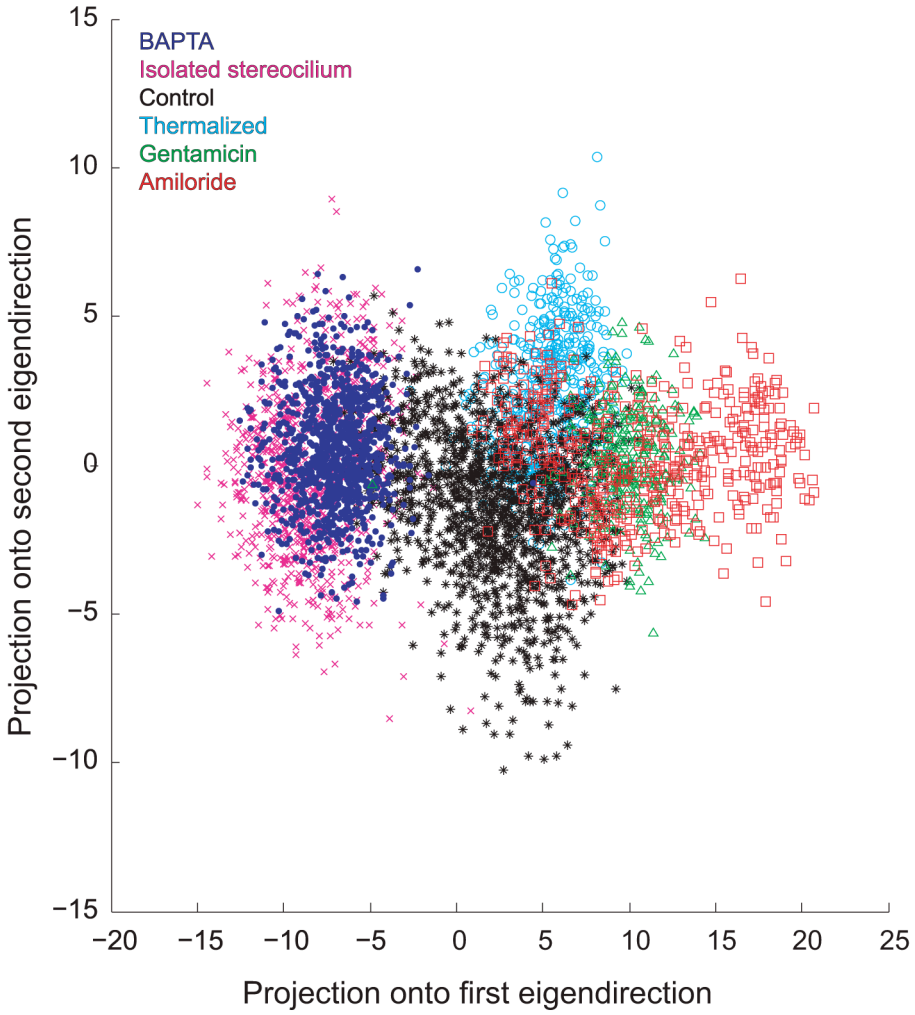

Figure S5. Clustering of records by treatment type. The power spectra for individual records were projected onto the first two principal components of a kernel principal components analysis. We were able to find convincing clustering with a simple linear kernel.

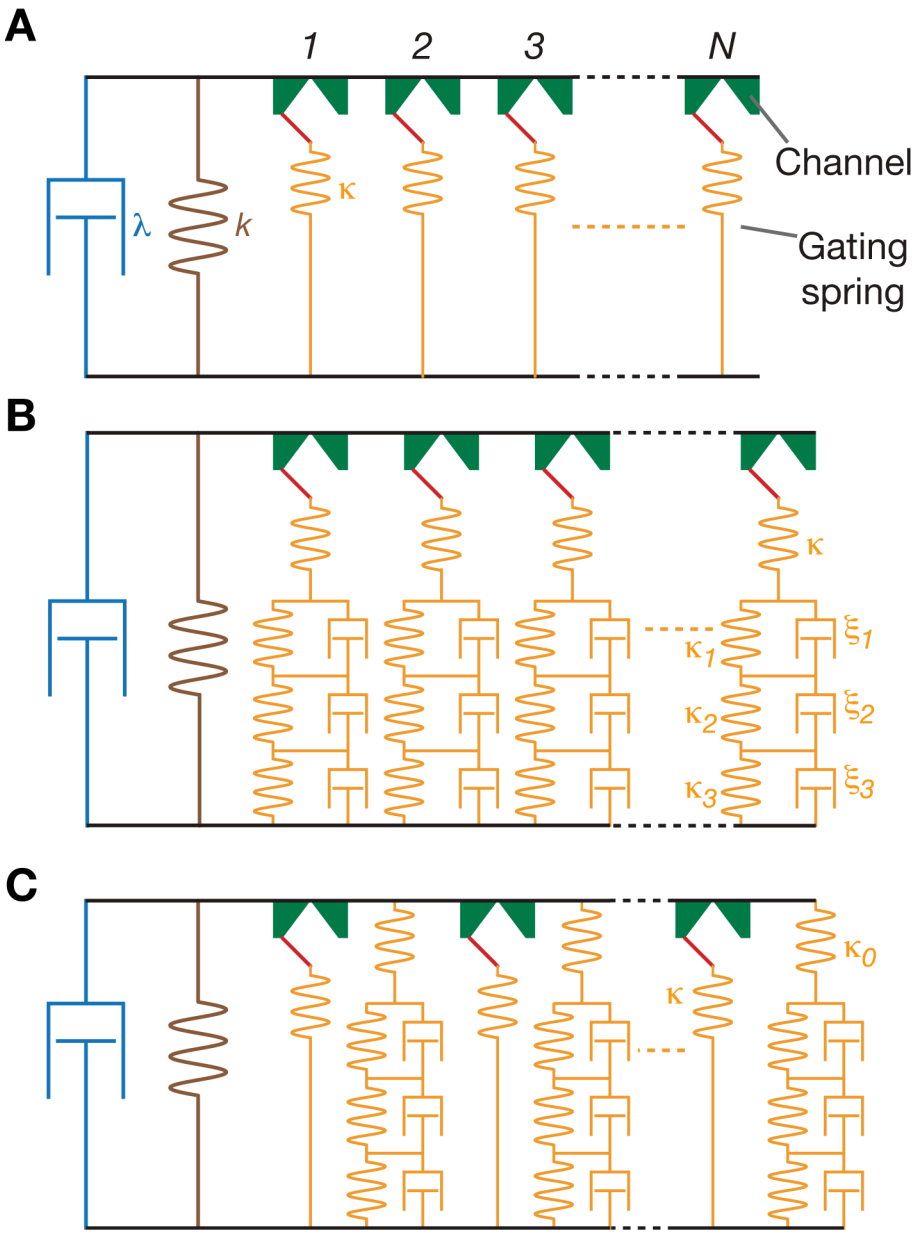

Figure S6. Models of the hair bundle's viscoelasticity. (*A*) In a mechanical representation of the canonical gating-spring model of a hair bundle, the gating springs are purely elastic and the only damping arises from the surrounding liquid. Each channel is depicted with a red gate attached to the associated gating spring. (*B*) An extended model with series viscoelasticity incorporates viscosity into the gating springs. (*C*) An alternative version of the extended model places the viscoelastic elements in parallel with the gating springs.

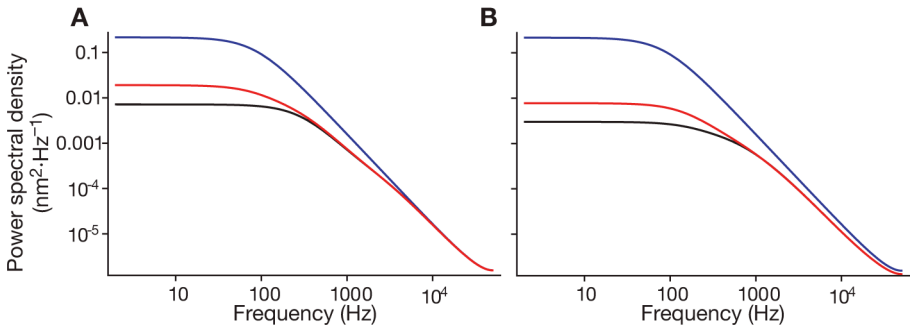

Figure S7. Subdiffusion from a parallel arrangement. (*A*) Power spectra are shown for viscoelastic modes arranged in series, with $\kappa = 1260$ μN·m^{-1}, $\kappa_1 = 700$ μN·m^{-1}, $\xi_1 = 260$ nN·s·m^{-1}, and $d = 4.1$ nm. (*B*) Similar spectra arise from viscoelastic modes arranged in parallel (Fig. S6C), with $\kappa = 800$ μN·m^{-1}, $\kappa_0 = 3.8$ μN·m^{-1}, $\kappa_1 = 38$ μN·m^{-1}, $\xi_1 = 200$ nN·s·m^{-1}, $d = 3.1$ nm, and $\tau = 0.4$ ms. The other parameter values and colors are those of Fig. 2 in the main text.

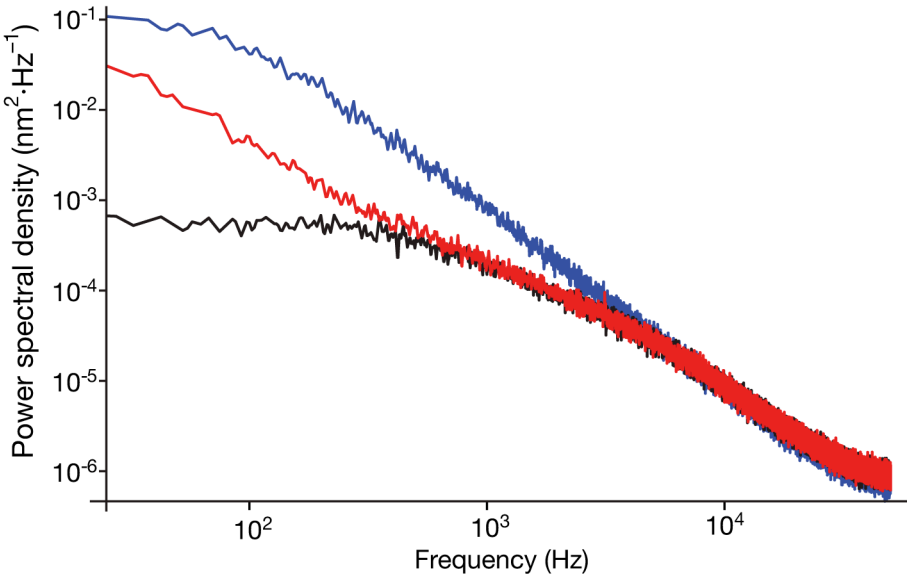

Figure S8. Demonstration of subdiffusion arising from systematic variation of a viscoelastic mode. The power spectrum was estimated for an ensemble of $j = 1,...,50$ channels whose mode structure was varied by holding all damping coefficients constant and changing the stiffnesses as $j^{1.12}$. The other parameter values and colors are those of Fig. 2 in the main text.